Nanoscale

RSC Publishing

PAPER

View Article Online
View Journal



Cite this: DOI: 10.1039/c3nr03097k

# A highly oriented hybrid microarray modified electrode fabricated by a template-free method for ultrasensitive electrochemical DNA recognition†

Lei Shi,[a] Zhenyu Chu,[a] Xueliang Dong,[a] Wanqin Jin*[a] and Eithne Dempsey[b]

Highly oriented growth of a hybrid microarray was realized by a facile template-free method on gold substrates for the first time. The proposed formation mechanism involves an interfacial structure-directing force arising from self-assembled monolayers (SAMs) between gold substrates and hybrid crystals. Different SAMs and variable surface coverage of the assembled molecules play a critical role in the interfacial directing forces and influence the morphologies of hybrid films. A highly oriented hybrid microarray was formed on the highly aligned and vertical SAMs of 1,4-benzenedithiol molecules with rigid backbones, which afforded an intense structure-directing power for the oriented growth of hybrid crystals. Additionally, the density of the microarray could be adjusted by controlling the surface coverage of assembled molecules. Based on the hybrid microarray modified electrode with a large specific area (*ca.* 10 times its geometrical area), a label-free electrochemical DNA biosensor was constructed for the detection of an oligonucleotide fragment of the avian flu virus H5N1. The DNA biosensor displayed a significantly low detection limit of 5 pM ($S/N = 3$), a wide linear response from 10 pM to 10 nM, as well as excellent selectivity, good regeneration and high stability. We expect that the proposed template-free method can provide a new reference for the fabrication of a highly oriented hybrid array and the as-prepared microarray modified electrode will be a promising paradigm in constructing highly sensitive and selective biosensors.

Received 16th June 2013
Accepted 16th August 2013

DOI: 10.1039/c3nr03097k

www.rsc.org/nanoscale

## Introduction

Highly sensitive and selective DNA biosensors constructed using facile approaches have attracted much attention in gene sequencing, forensic investigation, medical diagnostics, and environmental monitoring.[1,2] Consequently, a wide variety of DNA biosensors based on different detection strategies have been developed recently, which are mainly based on electrical, optical and piezoelectric-transduction techniques.[3–7] Considering the advantages of simplicity, cost, portability, and particularly ease of miniaturization, electrochemical methods have become one of the most attractive techniques in the development of DNA biosensors.[8,9]

Micro/nanostructures with large specific surface areas have received enormous interest in the application of chemical and biological sensors,[10–13] owing to their unique chemical and physical properties that cannot be achieved by the bulk materials. The enhanced surface area may provide more binding sites for the functional molecules and reaction positions for interfacial reactions, which would facilitate the acquisition and transmission of the signals and finally contribute to the increased sensitivity. As one of the most familiar structures, a micro/nanoarray is usually designed and fabricated for realizing the purpose of improving the specific surface area. Andreu *et al.* presented a nanowire array for DNA biosensing, in which they addressed the problems of the miniaturization of the electrode system and the increase of surface area.[14] Jagerszki *et al.* fabricated a gold nanotube modified electrode, which was used in a label-free DNA assay reaching a detection limit of 0.1 nM.[15] Feng *et al.* constructed a well-ordered nanoporous gold array with a large specific area for the detection of oligodeoxynucleotides and obtained a detection limit of approximately 10 fM.[16] In addition, Ramulu *et al.* prepared a gold nanowire array electrode, which showed enhanced electrochemical detection of nucleic acids with a detection limit of 6.78 nM.[17] Furthermore, Jamal *et al.* successfully synthesized a vertically aligned nickel

[a]*State Key Laboratory of Materials-Oriented Chemical Engineering, College of Chemistry and Chemical Engineering, Nanjing University of Technology, Nanjing 210009, P. R. China. E-mail: wqjin@njut.edu.cn; Fax: +86-25-8317-2292; Tel: +86-25-8317-2266*

[b]*Centre for Research in Electroanalytical Technologies (CREATE), Department of Science, Institute of Technology Tallaght, Tallaght, Dublin 24, Ireland*

† Electronic supplementary information (ESI) available: Four-probe method for determining the conductivity of the hybrid crystal (Fig. S1); stability comparisons of the hybrid films (Fig. S2); FESEM images of the hybrid microarray (Fig. S3); electrochemical characterizations of the hybrid films (Fig. S4); DFT simulations (Fig. S5); cross-sectional FESEM image of the hybrid microarray (Fig. S6); regeneration and stability tests of the DNA biosensor (Fig. S7). See DOI: 10.1039/c3nr03097k

nanowire array and Pt coated nickel nanowire for the sensitive detection of glutamate.[18] The introduction of the functional micro/nanoarray significantly improves the specific surface area of the fabricated biosensors and efficiently enhances their performances, and various templates (*e.g.* polycarbonate membrane, anodic aluminum oxide and porous silicon) are usually required during the fabrication of these structures. However, some drawbacks may exist in the fabrication process because the template synthesis suffers from complicated preparation of the templates, together with the difficulty in the removal of the template completely without compromising the integrity of the obtained structures. Therefore, new and facile preparation methods are expectative for the preparation of the desired micro/nanoarray.

In the past few years, on account of their chemical and structural diversity, uniform channels, thermal stability and ability to be chemically tailored, inorganic–organic hybrid materials have found many significant applications in gas adsorption and separation, catalysis and chemical sensors,[19–22] as well as ferroelectricity investigated in our previous work.[23,24] Apart from their use as bulk materials, the preparation of thin films of these hybrid materials, especially with oriented structures, is a prerequisite and is stimulated by the enormous demand in practical applications, *e.g.* electrochemical sensors, micro/nano devices and smart membranes.[25,26] However, unlike inorganic materials, inorganic–organic hybrid materials possess some particular characteristics, *e.g.* the large and complex unit cells, which make it extraordinarily difficult to control the morphologies of hybrid films and similar structures of highly oriented arrays with a large specific area have not been reported.

In this work, a highly oriented hybrid microarray of Ni-$(en)_3Ag_2I_4$ (where en represents diaminoethane) was fabricated by a template-free method on a gold substrate, in which SAMs with rigid backbones were introduced to afford the powerful structure-directing force for the oriented growth of hybrid crystals. The influence of SAMs with different conformations and surface coverage on the morphologies of obtained hybrid films was investigated. Based on the oriented hybrid microarray modified electrode with a large specific area, a label-free electrochemical DNA biosensor was successfully constructed for the detection of an oligonucleotide fragment of the avian flu virus H5N1, which showed a significantly low detection limit and excellent selectivity.

## Experimental section

### Chemicals and materials

All oligonucleotides were synthesized and purified by Sangon Inc. (Shanghai, China). DNA probe: 5′-HS-$(CH_2)_6$-TTT GAG TCT GTT GCT TGG-3′, complementary target: 5′-CCA AGC AAC AGA CTC AAA-3′ (a fragment of the avian flu virus H5N1), single-base mismatched target: 5′-CCA AGC AAG AGA CTC AAA-3′, non-complementary target: 5′-AGT GTT CTT CTC ATC ATC-3′. 1,4-Benzenedithiol, 1,6-hexanedithiol, potassium ferricyanide ($K_3Fe(CN)_6$), tris(hydroxymethyl)aminomethane (Tris-base), hexaammineruthenium(III) chloride (RuHex) and 6-mercapto-1-hexanol (MCH) were obtained from Sigma-Aldrich. Hydrochloric acid (HCl), silver nitrate ($AgNO_3$), potassium iodide (KI), nickel nitrate ($Ni(NO_3)_2 \cdot 6H_2O$), *N*,*N*-dimethylformamide (DMF), 1,2-ethylenediamine and ethanol were purchased from Sinopharm Chemical Reagent Co., Ltd. DNA immobilization buffer: 10 mM Tris–HCl, 1 mM EDTA, 10 mM TCEP, and 0.1 M NaCl (pH 7.4). Hybridization buffer: 10 mM phosphate buffered solution (PBS, pH 7.4) with 0.25 M NaCl. Washing buffer was 10 mM Tris–HCl (pH 7.4). All solutions were prepared with MilliQ water (18 MΩ $cm^{-1}$).

### Formation of hybrid films on gold substrates

Gold thin film electrodes with a diameter of 1 mm were pretreated by following a known procedure.[27] The freshly cleaned gold electrodes were immersed into a 5 mM 1,4-benzenedithiol or 1,6-hexanedithiol ethanolic solution for different time periods ranging from 2 h to 10 h to form the SAMs, which were subsequently rinsed with ethanol.

The preparation of the hybrid mother solution was reported elsewhere.[28] Here special treatments of the solution were required: the mother solution was maintained at 80 °C for 72 h, heated to 100 °C for 24 h, and then cooled to 25 °C.

The hybrid solution was filtered first, and then the gold electrodes were dipped vertically into the solution and finally allowed to crystallize at 25 °C.

### Thickness measurements of SAMs through ellipsometry

Ellipsometry is adopted to record the change in polarization of elliptically polarized light, when it reflects on the surface of SAM modified gold substrates. From the changes in the ellipsometric angles, the refractive index and the optical thickness of the SAM can be deduced.[29,30] The measurement was performed using a 632.8 nm line of a He/Ne laser incident upon the sample at 70°. The ellipsometric angles ($\Delta$, $\Psi$), were determined for both the bare clean substrate and the self-assembled film. The so-called DafIBM program supplied by Rudolph Technologies was employed to determine the thickness values, assuming that the refractive indices of the 1,4-benzenedithiol and 1,6-hexanedithiol organic films were 1.45 and 1.51 respectively.[31] At least five different sampling points were considered to obtain averaged thickness values.

### Construction of the DNA biosensor on the hybrid microarray modified electrode

The thiolated single-stranded DNA (ss-DNA) probes were immobilized by incubating the microarray modified electrode in the immobilization solution containing 5 μM probes at room temperature for different times (1–13 h). After unbound probes were washed away with distilled water, the unreacted active surface groups were subsequently passivated by reaction with 500 nM 6-mercapto-1-hexanol (MCH) solution for 2 h. The probe-attached microarray modified electrode was then immersed in the hybridization buffer containing a series of concentration of target strands for 4 h, which was then rinsed with washing buffer.

 

### Electrochemical measurements

All electrochemical measurements were performed with a CHI 660C electrochemical workstation (Shanghai Chenhua, China). A conventional three-electrode configuration was employed during the experiment, which involved a working electrode (the hybrid microarray modified gold electrode), a platinum auxiliary electrode, and an Ag/AgCl (saturated KCl) reference electrode. The square wave voltammetric (SWV) measurements were taken at a frequency of 5 Hz, and chronocoulometry (CC) measurements were conducted at a pulse width of 0.25 s. The electrolyte for SWV was 5 mM $Fe(CN)_6^{3-}$ and 250 mM NaCl, and for CC was 10 mM Tris–HCl (pH 7.4). During the CC measurement, a nitrogen atmosphere was maintained in the electrochemical cell.

## Results and discussion

### Structures and properties of the hybrid material

The hybrid material, with a formula of $Ni(en)_3Ag_2I_4$, crystallizes in the hexagonal space group $P6_3$ and its crystal structure is displayed in Fig. 1. An asymmetric unit contains two crystallographically different $Ag^+$ ions (labeled Ag1 and Ag2), two crystallographically inequivalent $I^-$ anions (labeled I1 and I2), one $Ni^{2+}$ ion together with one diaminoethane ligand (Fig. 1a). The Ag1, Ag2 and I2 ions occupy the 2b Wyckoff positions; the Ni1 ion occupies the 2a Wyckoff position; the I1 ion and the C1, C2, N1 and N2 atoms in the diaminoethane ligand occupy the general positions. The Ag1 and Ag2 ions are correspondingly bound to one I2-type and three I1-type iodide ions to form two types of $AgI_4$ tetrahedral coordination spheres with a $C_3$ point-group symmetry. Two types of $AgI_4$ tetrahedra share a vertex; each Ag1-type $AgI_4$ tetrahedron is surrounded by four Ag2-type $AgI_4$ tetrahedra and *vice versa*. The three-dimensional $\{Ag_2I_4^{2-}\}_\infty$ framework, which consists of $AgI_4$ tetrahedra, is shown in Fig. 1b, projected along the crystallographic *c*-axis. The $Ni^{2+}$ ion is coordinated to six N atoms, which belong to three diaminoethane molecules, to form an octahedral coordination sphere with a $C_3$ point-group symmetry. Such mononuclear species are filled in the cavity of the 3-D $\{Ag_2I_4^{2-}\}_\infty$ framework (Fig. 1c).

The unique framework of the $\{Ag_2I_4^{2-}\}_\infty$ structure imparts some novel properties of photons and electrons to this hybrid material. The electrical conductivity of a single crystal was examined using the four-probe method (Fig. S1 in the ESI†) and a conductivity of $8.9 \times 10^{-4}$ S $cm^{-1}$ was obtained at room temperature. Such a high conductivity facilitates the applications of this hybrid material in electrochemistry.[32] In addition, this material shows two other fascinating features: high chemical stability in a phosphate buffer saline (PBS) of pH = 6.8–7.8 and robust resistance to ambient illumination compared with silver iodide (AgI). Especially, on account of regularly distributed Ag ions in the hybrid framework, the hybrid material could serve as a promising substrate for the regular immobilization of thiolated biomolecule probes through Ag–S bonds,[33,34] which was favorable for rationalizing and controlling the distribution of biomolecule probes.

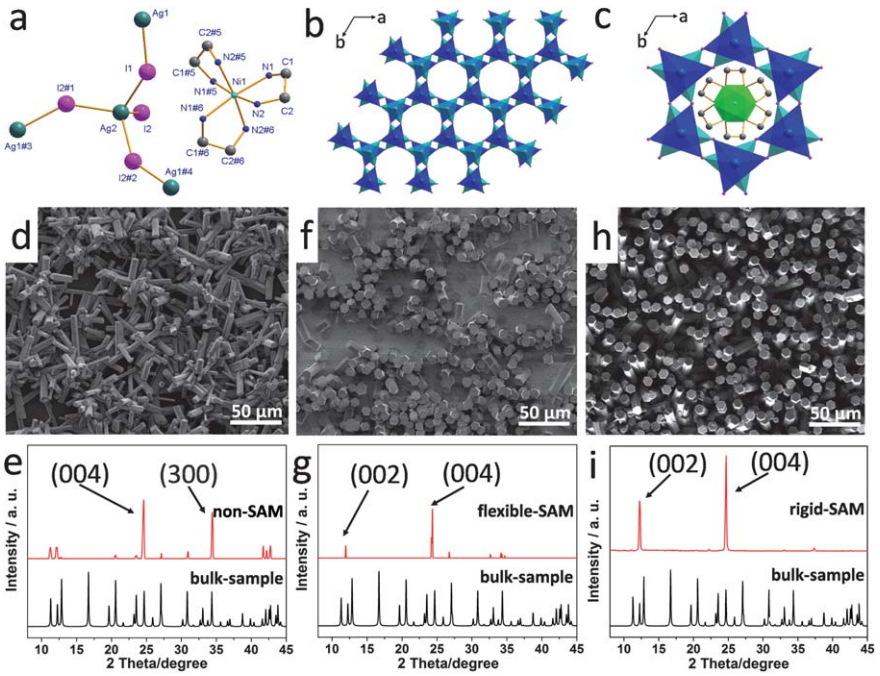


**Fig. 1** (a) An asymmetric unit of $Ni(en)_3Ag_2I_4$ (the hydrogen atoms in the diaminoethane ligands are omitted for clarity, and the atoms marked with # are at the following symmetry positions: #1 = 1 − *x* + *y*, 1 − *x*, *z*; #2 = 1 − *y*, *x* − *y*, *z*; #3 = −1 + *x*, −1 + *y*, *z*; #4 = −1 + *x*, *y*, *z*; #5 = 1 − *x* + *y*, 2 − *x*, *z*; #6 = 2 − *y*, 1 + *x* − *y*, *z*). (b) The 3-D $\{Ag_2I_4\}_\infty$ framework in the crystal of $Ni(en)_3Ag_2I_4$, projected along the crystallographic *c*-axis. (c) Illustration of $Ni(en)_3^{2+}$ ions filled in the cavity of the 3-D $\{Ag_2I_4\}_\infty$ framework. (d), (f) and (h) FESEM images of hybrid films with different morphologies on bare gold substrates, 1,6-hexanedithiol modified gold substrates and 1,4-benzenedithiol modified gold substrates respectively. (e), (g) and (i) X-ray diffraction patterns corresponding to (d), (f) and (h).

### Fabrication of hybrid films on gold substrates

Gold substrates for the growth of hybrid films were modified with SAMs of 1,4-benzenedithiol and 1,6-hexanedithiol to create an artificial organic interface respectively. One terminal –SH group of the SAMs was anchored onto the surface of the gold substrate *via* an Au–S bond, while the other terminal –SH group was expected to bind with Ag ions of the hybrid crystal. As shown in Fig. 1d, f and h, the disordered hybrid microcrystals were grown on the bare gold substrates with various sizes of single crystals (ref. Fig. 1d); the local domains of the microarray were observed on the gold surfaces when 1,6-hexanedithiol was used (see Fig. 1f), and the highly integrated and homogeneous hybrid microarray, consisting of the hexagonal prism-shaped crystals with an average side length of *ca.* 5 μm, was obtained on the 1,4-benzenedithiol modified gold surfaces (see Fig. 1h). For this oriented hexagonal prism-shaped microarray, only two Bragg reflections indexed as (0 0 2) and (0 0 4) appeared in the XRD profile (Fig. 1i), indicating that the hybrid microarray grown on the 1,4-benzenedithiol SAMs was highly oriented along the crystallographic [001] direction.

The crystal shape and size are controllable *via* tuning the crystal growth time. Transmission electron microscopy (TEM) was performed to monitor the growth of hexagonal prisms, as shown in Fig. 2. In the initial 4 hours, an analogous cylinder with a side length of 1 μm and a height of 8 μm was observed (Fig. $2a_{1,2}$). Then hexagonal prisms with defects on the surface were subsequently obtained after the sample was incubated for an additional 3 hours (Fig. $2b_{1,2}$). Finally, a perfect structure of a hexagonal prism was obtained with more crystallization time of up to 10 hours (Fig. $2c_{1,2}$). It is worth mentioning that the intact crystal structure was critical for the stability of the fabricated microcrystals, especially in the PBS solution (Fig. S2 in the ESI†).

In addition, the effect of different surface coverages of 1,4-benzenedithiol molecules on the morphologies of the hybrid microarray was investigated. As the gold substrates were immersed in the 1,4-benzenedithiol solution for various time periods of 2 h, 6 h and 10 h respectively, different distribution densities of the hybrid microarray were observed on the gold substrates (Fig. S3 in the ESI†). The results showed that a sparse microarray was obtained at a low coverage of 1,4-benzenedithiol SAMs, while a crowded microarray was fabricated with a higher coverage. With an appropriate time of 6 h, a homogeneous microarray with moderate density was prepared. Considering that the surface area of the sparse microarray was limited, and the crowded microarray would not facilitate the diffusion profiles,[35,36] the microarray with moderate density on the gold substrate was selected for constructing the DNA biosensor (Fig. S4 in the ESI†).

### Formation mechanism of the hybrid microarray

It is understood that various SAMs affected the growth of hybrid films since different SAMs had distinct conformations formed on the same substrate.[37,38] Ellipsometry was introduced to measure the thickness of the formed SAMs. The results showed that the thicknesses of the 1,4-benzenedithiol and 1,6-hexanedithiol SAMs were $5.9 \pm 0.3$ and $4.1 \pm 0.2$ Å respectively (the physical lengths of these molecules are *ca.* 6.7 and 9.3 Å), which indicated that the disordered and flexible SAMs of 1,6-hexanedithiol were formed on the gold surface, while in the case of 1,4-benzenedithiol, significantly improved and relatively erect SAMs were obtained.[39,40] Similar conclusions could be confirmed from the Density Functional Theory (DFT) simulations, as shown in Fig. S5 in the ESI.† Since the –SH groups at the terminal of 1,4-benzenedithiol molecules are deemed to orient along [001],[41,42] the binding of –SH groups with Ag ions of the hybrid crystals will enable crystal growth only along the [001] direction to give the highly oriented hybrid microarray, which is schematically illustrated in Fig. 3. Meanwhile the higher coverage of the 1,4-benzenedithiol would provide more binding sites, leading to a more crowded distribution of hybrid microarray, while for the SAMs of 1,6-hexanedithiol with flexible backbones, both terminal –SH groups of partial 1,6-hexanedithiol molecules may anchor onto the gold surface and other molecules are prone to bend on the surface. Therefore the binding sites are reduced and the orientation-induced forces become weak, which made it difficult to obtain the integrated hybrid microarray on the gold surfaces. Because there was no agent on the bare gold substrates to induce the oriented growth of hybrid films, disordered hybrid microcrystals were obtained

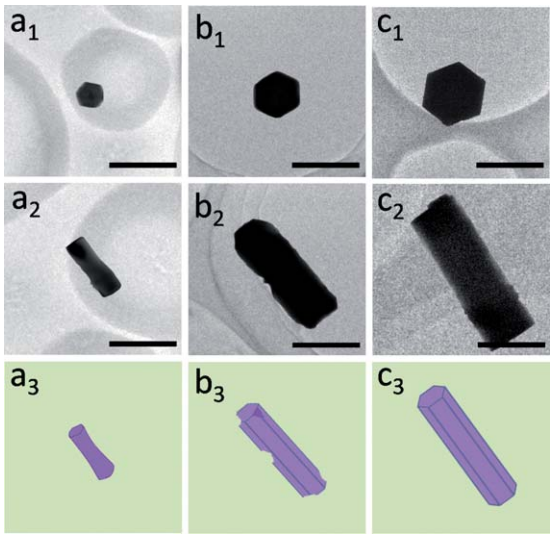


**Fig. 2** TEM images of hybrid hexagonal prisms incubated in the crystallization solution for (a) 4 h, (b) 7 h, and (c) 10 h; subscripts 1, 2 and 3 represent top views, cross-sections and schematic drawings respectively. The scale bar is 10 μm.

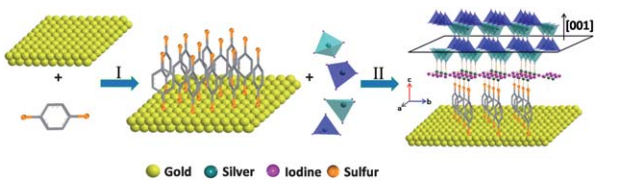


**Fig. 3** Schematic illustrations for the formation of the highly oriented hybrid microarray on the 1,4-benzenedithiol functionalized gold substrates. Hybrid crystals grow in the [001] direction.

under this condition. Furthermore, without the binding interactions from the SAMs, the obtained disordered microcrystals were prone to peeling from the gold surfaces.

### Optimization of experimental conditions in the DNA hybridization

Chronocoulometry (CC) was introduced to investigate the probe density and hybridization efficiency of the hybrid microarray modified electrode,[43,44] which is shown in Fig. 4. Hexaammineruthenium(III) chloride (RuHex) served as the electrochemical indicator in the CC experiments, which was stoichiometrically bound to the anionic phosphodiester backbone of DNA and therefore quantitatively reflected the amount of DNA strands on the surface. The influence of the concentration of RuHex on the CC charge was first studied, which is shown in Fig. 4a. As the concentration of RuHex improved from 10 μM to 100 μM, the probe density increased from $1.5 \times 10^{11}$ molecules per $cm^2$ to $4.1 \times 10^{12}$ molecules per $cm^2$. While the RuHex concentration was further increased to 150 μM, no obvious changes of the probe density were observed. The result indicated that 100 μM RuHex was the saturation concentration for the determination of the probe density in this study. The probe density and hybridization efficiency obtained with different incubation time were subsequently detected, as shown in Fig. 4b. With the incubation time ranging from 1 h to 13 h, the surface density of the probe increased from $1.4 \times 10^{10}$ molecules per $cm^2$ to $6.5 \times 10^{12}$ molecules per $cm^2$ while the hybridization efficiency decreased from 0.99 to 0.72. Considering that it was difficult to obtain well-defined electrochemical signals at both low surface density and hybridization efficiency,[44,45] an optimal incubation time of 7 h was selected and under this condition the probe density of $4.1 \times 10^{12}$ molecules per $cm^2$ with a high hybridization efficiency of 0.93 was observed.

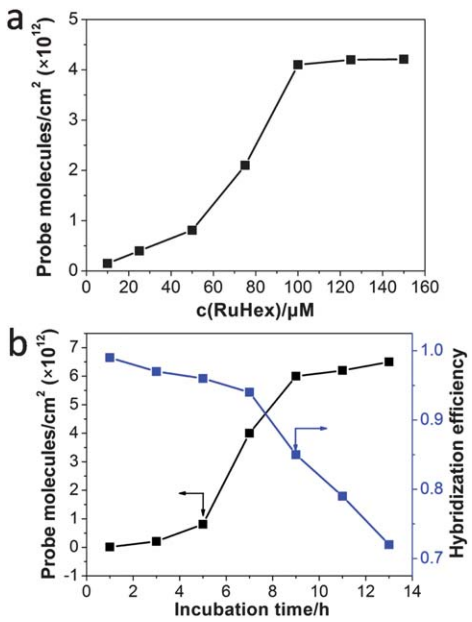


**Fig. 4** (a) Probe density on the surface of the hybrid microarray modified electrode measured with different RuHex concentrations of 10 μM, 25 μM, 50 μM, 75 μM, 100 μM, 125 μM and 150 μM respectively. (b) Probe density on the surface of the hybrid microarray incubated with a 5 μM DNA probe for different incubation time of 1 h, 3 h, 5 h, 7 h, 9 h, 11 h and 13 h respectively. The hybridization efficiency was measured after the hybridization with 1 μM target strands.

### DNA hybridization based on the hybrid microarray modified electrode

The $K_3Fe(CN)_6$ aqueous solution served as the electrochemical indicator to monitor the DNA hybridization. In the absence of the targets, the current–potential curve in the SWVs (Fig. 5a, black line) exhibited a reference electrochemical signal, and this situation was designated as the 'OFF' state. When the probes were hybridized with the targets at a concentration of 10 nM, a notable increment of the response current was observed (Fig. 5a, red line), which was designated as the 'ON' state.

Based on this 'OFF'/'ON' phenomenon, the sensitivity curves for DNA hybridization based on hybrid films with various

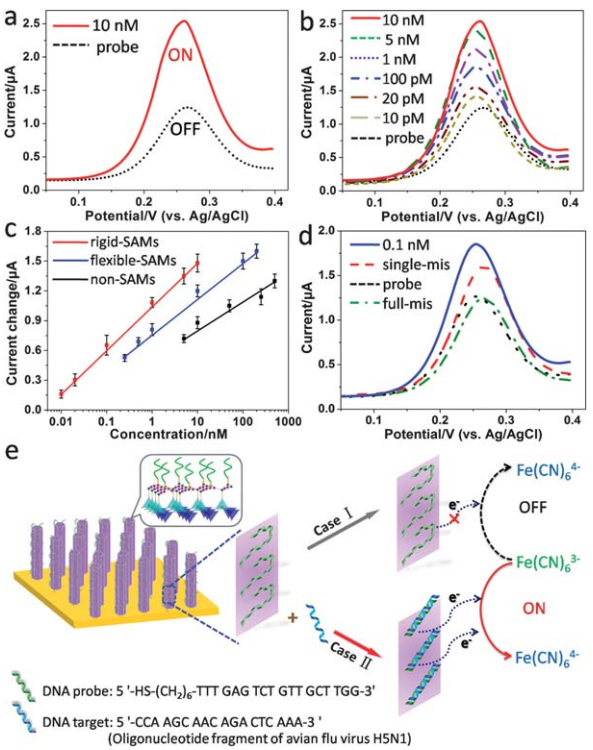


**Fig. 5** (a) SWVs of 5 mM $Fe(CN)_6^{3-}$ at the DNA probe attached highly oriented hybrid microarray before (designated as the 'OFF' state) and after hybridization with 10 nM target (designated as the 'ON' state). (b) SWVs of 5 mM $Fe(CN)_6^{3-}$ at the hybrid microarray after hybridization with complementary targets of various concentrations. An ultrasensitive detection limit of 5 pM was obtained. (c) Calibration sensitivity curves of the peak value changes *versus* the target concentrations based on hybrid films with different morphologies fabricated on bare gold substrates, flexible SAM and rigid SAM modified gold substrates respectively; the responses were logarithmically related to target concentrations. (d) SWVs of 5 mM $Fe(CN)_6^{3-}$ at the hybrid microarray before and after hybridization with complementary, non-complementary and single-base mismatched DNA strands at a concentration of 0.1 nM respectively. (e) Schematic illustrations of the 'OFF'/'ON' mechanism on the surface of the DNA-attached hybrid microarray.

morphologies were further investigated and compared using SWVs. By varying the concentrations of complementary targets, different detection limits of 4 nM, 150 pM and 5 pM (3 times the signal-to-noise ratio, Fig. 5b and c) were achieved for hybrid films fabricated on the bare gold surfaces, flexible SAM and rigid SAM modified gold substrates respectively. In the case of disordered hybrid films, the specific surface area was limited. The interlaced structure of hybrid films reduced the effective immobilization sites for DNA probes and increased the interference amongst DNA strands on the adjacent hybrid crystals, which might affect the interfacial transfer of $Fe(CN)_6^{3-}$ and disturb the recognition of the response signal. Therefore a high detection limit with smaller changes in the response signal was observed for the disordered hybrid film modified electrode. In contrast, the hybrid microarray possesses an enhanced specific surface area compared with disordered hybrid films, which could provide more binding sites and reduce the interference arising from the DNA strands on the adjacent array. Accordingly, an improved detection performance was achieved for the hybrid film fabricated on the flexible SAM modified gold substrates. When the integrated and homogeneous hybrid microarray was synthesized on the rigid SAM modified gold surfaces, a larger specific area (approximately ten times its geometrical area, shown in Fig. S6 in the ESI†) was obtained, which significantly enhanced the mass transport and facilitated the acquisition of signals, resulting in an ultrasensitive detection limit with distinct electrochemical signal responses. Considering the omission of the cumbersome labeling of DNA strands and the simple electrochemical detection system, the 5 pM performance of this DNA sensor was distinctly superior to other comparable sensors (typically 0.1–10 nM).[15,46–49] Moreover, the specific recognition to DNA sequences based on the microarray modified electrode was performed with the non-complementary and single-base mismatched target strands respectively (Fig. 5d). The results indicated that this DNA biosensor could distinctly discriminate targets with a single mismatched base even at a low concentration.

### Regeneration and stability of the fabricated DNA biosensor

The regeneration and stability of a DNA biosensor are extremely important for practical applications. It was observed that the fabricated DNA biosensor could be regenerated 8 times with about 18% loss of the original signal changes (Fig. S7a in the ESI†) by dipping the modified electrode in hot water (80 °C) for 15 min, followed by rapid cooling in an ice bath for 10 min.[44] The signal attenuation may be due to the loss of probe strands on the electrode surface. In addition, the probe-attached electrode was first stored in the refrigerator at 4 °C for 5 days, 10 days and 15 days respectively, and then examined after the hybridization. Experiments demonstrated that the DNA biosensor retained about 95% of its initial response changes even after 15 days (Fig. S7b in the ESI†).

### Proposed mechanism for the 'OFF'/'ON' phenomenon

A possible mechanism to produce the 'OFF'/'ON' phenomenon is proposed, as illustrated in Fig. 5e. The single-stranded DNA (ss-DNA) molecule is a flexible polymer, and it is prone to lie on the surface of the hybrid microarray modified electrode. The hybridized double-stranded DNA (ds-DNA) molecule, in contrast, is a rigid polymer and it favors an upright configuration.[50–52] In the 'OFF' state, the flexible ss-DNA probes that cover the surface of the hybrid microarray block the interfacial electron transfer from $Fe(CN)_6^{3-}$ to the electrode surface (case I) because the DNA molecule with anionic phosphodiester groups in the backbone is a negatively charged polyelectrolyte. In the 'ON' state, upon the formation of ds-DNA *via* hybridization with the target strands, the rigid DNA duplex stands upright at the surface of the microarray, which significantly increases the accessibility of $Fe(CN)_6^{3-}$ to the electrode surface and leads to a distinct change of electrochemical signals (case II).

## Conclusions

In summary, we have reported a highly oriented growth of a $Ni(en)_3Ag_2I_4$ hybrid microarray with a template-free method on gold substrates. The different configurations and surface coverage of the formed SAMs played critical roles in the morphologies of the obtained hybrid films. Based on the oriented hybrid microarray modified electrode, a label-free electrochemical DNA biosensor was designed and a possible 'OFF'/'ON' mechanism was proposed for the hybridization process. The fabricated biosensor showed a significantly enhanced detection limit of 5 pM, excellent selectivity, good regeneration and high stability. We hope that the proposed template-free method can provide a new reference for the fabrication of an oriented hybrid array and the as-prepared microarray modified electrode will be a promising paradigm in constructing highly sensitive and selective biosensors.

## Acknowledgements

This work was supported by the National Natural Science Foundation of China (no. 21176115), Doctoral Fund of Ministry of Education of China (20113221110001), and Innovation Foundation for Doctoral Dissertation of Jiangsu Province (CXLX12_0443). We sincerely thank Prof. Xiaoming Ren for his assistance with the optimization of conditions in the preparation of hybrid material films and helpful discussions.

## Notes and references

1 J. Liu, Z. Cao and Y. Lu, *Chem. Rev.*, 2009, **109**, 1948.
2 A. A. Lubin and K. W. Plaxco, *Acc. Chem. Res.*, 2010, **43**, 496.
3 L. Soleymani, Z. C. Fang, E. H. Sargent and S. H. Kelley, *Nat. Nanotechnol.*, 2007, **4**, 844.
4 L. Shi, Z. Chu, Y. Liu, W. Jin and X. Chen, *Biosens. Bioelectron.*, 2013, **49**, 184.
5 C. Y. Zhang, H. C. Yeh, M. T. Kuroki and T. H. Wang, *Nat. Mater.*, 2005, **4**, 826.
6 Y. Wen, L. Xu, W. Wang, D. Wang, H. Du and X. Zhang, *Nanoscale*, 2012, **4**, 4473.
7 F. Patolsky, A. Lichtenstein and I. Willner, *Chem.–Eur. J.*, 2003, **9**, 1137.

 

8 T. G. Drummond, M. G. Hill and J. K. Barton, *Nat. Biotechnol.*, 2003, **21**, 1192.
9 C. Batchelor-McAuley, G. G. Wildgoose and R. G. Compton, *Biosens. Bioelectron.*, 2009, **24**, 3183.
10 C. N. LaFratta and D. R. Walt, *Chem. Rev.*, 2008, **108**, 614.
11 N. J. Wittenberg, H. Im, T. W. Johnson, X. H. Xu, A. E. Warrington, M. Rodriguez and S. H. Oh, *ACS Nano*, 2011, **5**, 7555.
12 X. J. Huang, A. M. O'Mahony and R. G. Compton, *Small*, 2009, **5**, 776.
13 B. Sljukić, C. E. Banks and R. G. Compton, *Nano Lett.*, 2006, **6**, 1556.
14 A. Andreu, J. W. Merkert, L. A. Lecaros, B. L. Broglin, J. T. Brazell and M. El-Kouedi, *Sens. Actuators, B*, 2006, **114**, 1116.
15 G. Jagerszki, B. E. Gyurcsanyi, L. Hofler and E. Pretsch, *Nano Lett.*, 2007, **7**, 1609.
16 J. Feng, W. Zhao, B. Su and J. Wu, *Biosens. Bioelectron.*, 2011, **30**, 21.
17 T. S. Ramulu, R. Venu, B. Sinha, B. Lim, S. J. Jeon, S. S. Yoon and C. G. Kim, *Biosens. Bioelectron.*, 2013, **40**, 258.
18 M. Jamal, M. Hasan, A. Mathewson and K. M. Razeeb, *Biosens. Bioelectron.*, 2013, **40**, 213.
19 S. Kitagawa, R. Kitaura and S. I. Noro, *Angew. Chem., Int. Ed.*, 2004, **43**, 2334.
20 D. B. Dang, P. Y. Wu, C. He, Z. Xie and C. Y. Duan, *J. Am. Chem. Soc.*, 2010, **132**, 14321.
21 G. Lu and J. T. Hupp, *J. Am. Chem. Soc.*, 2010, **132**, 7832.
22 B. V. Harbuzaru, A. Corma, F. Rey, P. Atienzar, J. L. Jorda, H. Garcia, D. Ananias, L. D. Carlos and J. Rocha, *Angew. Chem., Int. Ed.*, 2008, **47**, 1080.
23 C. Pan, J. P. Nan, X. L. Dong, X. M. Ren and W. Q. Jin, *J. Am. Chem. Soc.*, 2011, **133**, 12330.
24 H. R. Zhao, D. P. Li, X. M. Ren, Y. Song and W. Q. Jin, *J. Am. Chem. Soc.*, 2010, **132**, 18.
25 O. Shekhah, J. Liu, R. A. Fischer and C. WÖll, *Chem. Soc. Rev.*, 2011, **40**, 1081.
26 A. Betard and R. A. Fischer, *Chem. Rev.*, 2012, **112**, 1055.
27 J. Zhang, S. P. Song, L. H. Wang, D. Pan and C. H. Fan, *Nat. Protoc.*, 2007, **2**, 2888.
28 Y. S. Jiang, H. G. Yao, S. H. Ji, M. Ji and Y. L. An, *Inorg. Chem.*, 2008, **47**, 3922.
29 F. Hook and B. Kasemo, *Anal. Chem.*, 2001, **73**, 5796.
30 S. W. Joo, S. W. Han and K. Kim, *J. Colloid Interface Sci.*, 2001, **201**, 391.
31 C. D. Bain, E. B. Troughton, Y. T. Tao, J. Evall, G. M. Whitesides and R. G. Nuzzo, *J. Am. Chem. Soc.*, 1989, **111**, 321.
32 L. F. Yang, S. Kinoshita, T. Yamada, S. Kanda, H. Kitagawa, M. Tokunaga, T. Ishimoto, T. Ogura, R. Nagumo, A. Miyamoto and M. Koyama, *Angew. Chem., Int. Ed.*, 2010, **49**, 5348.
33 H. I. Peng, C. M. Strohsahl, K. E. Leach, T. D. Krauss and B. L. Miller, *ACS Nano*, 2009, **3**, 2265.
34 Y. Wen, W. Wang, Z. Zhang, L. Xu, H. Du, X. Zhang and Y. Song, *Nanoscale*, 2013, **5**, 523.
35 D. Menshykau, X. J. Huang, N. V. Rees, F. J. del Campo, F. X. Munozb and R. G. Compton, *Analyst*, 2009, **134**, 343.
36 T. J. Davies and R. G. Compton, *J. Electroanal. Chem.*, 2005, **585**, 63.
37 J. C. Love, L. A. Estroff, J. K. Kriebel, R. G. Nuzzo and G. M. Whitesides, *Chem. Rev.*, 2005, **105**, 1103.
38 R. Arnold, W. Azzam, A. Terfort and C. WÖll, *Langmuir*, 2002, **18**, 3980.
39 S. Flink, F. C. J. M. van Veggel and D. N. Reinhoudt, *Adv. Mater.*, 2000, **12**, 1315.
40 M. A. Reed, C. Zhou, C. J. Muller, T. P. Burgin and J. M. Tour, *Science*, 1997, **278**, 252.
41 A. Schoedel, C. Scherb and T. Bein, *Angew. Chem., Int. Ed.*, 2010, **49**, 7225.
42 C. Scherb, A. Schodel and T. Bein, *Angew. Chem., Int. Ed.*, 2008, **47**, 5777.
43 A. B. Steel, T. M. Herne and M. J. Tarlov, *Anal. Chem.*, 1998, **70**, 4670.
44 J. Zhang, S. P. Song, L. Y. Zhang, L. H. Wang, H. P. Wu, D. Pan and C. H. Fan, *J. Am. Chem. Soc.*, 2006, **128**, 8575.
45 R. J. Lao, S. P. Song, H. P. Wu, L. H. Wang, Z. Z. Zhang, L. He and C. H. Fan, *Anal. Chem.*, 2005, **77**, 6475.
46 G. Liu, C. F. Sun, D. Li, S. P. Song, B. W. Mao, C. H. Fan and Z. Q. Tian, *Adv. Mater.*, 2010, **22**, 1.
47 H. Aoki, P. Buhlmann and Y. Umezawa, *Electroanalysis*, 2000, **12**, 1272.
48 S. J. Li, J. Li, K. Wang, C. Wang, J. J. Xu, H. Y. Chen, X. H. Xia and Q. A. Huo, *ACS Nano*, 2010, **4**, 6417.
49 P. Kohli, C. C. Harrell, Z. H. Cao, R. Gasparac, W. H. Tan and C. R. Martin, *Science*, 2004, **305**, 984.
50 T. M. Herne and M. J. Tarlov, *J. Am. Chem. Soc.*, 1997, **119**, 8916.
51 C. H. Fan, K. W. Plaxco and A. J. Heeger, *Proc. Natl. Acad. Sci. U. S. A.*, 2003, **100**, 9134.
52 D. Y. Petrovykh, V. Perez-Dieste, A. Opdahl, H. Kimura-Suda, J. M. Sullivan, M. J. Tarlov, F. J. Himpsel and L. J. Whitman, *J. Am. Chem. Soc.*, 2006, **128**, 2.